NASA SP-53

A QUASI-GLOBAL PRESENTATION OF TIROS III RADIATION DATA

NATIONAL AERONAUTICS AND SPACE ADMINISTRATION

NASA SP-53

A QUASI-GLOBAL PRESENTATION OF TIROS III RADIATION DATA

by

LEWIS J. ALLISON
Goddard Space Flight Center

THOMAS I. GRAY, JR.
U. S. Weather Bureau

GUENTER WARNECKE*
Goddard Space Flight Center

prepared by

GODDARD SPACE FLIGHT CENTER, GREENBELT, MARYLAND

* On leave from the Institut für Meteorologie und Geophysik der Freien Universität Berlin, Berlin, Germany, as a National Academy of Sciences–National Research Council Research Associate with the National Aeronautics and Space Administration.

For sale by
the Superintendent of Documents,
U.S. Government Printing Office
Washington, D.C. 20402
Price $2.00 (Paper Cover)

Scientific and Technical Information Division 1964
NATIONAL AERONAUTICS AND SPACE ADMINISTRATION
Washington, D. C.

FOREWORD

Perhaps the most significant aspect of the meteorological satellite is its inherent ability to obtain routine coverage of the entire globe. Although much has been written about the operational use of satellite television pictures, relatively little has been said about the synoptic use of radiation data.

As a step toward rectifying this imbalance, the authors of this paper present a worldwide radiation map in the 8 to 12 micron atmospheric "window" and discuss in detail the large-scale synoptic application of the infrared data. An extra large format is employed to facilitate the reader's grasp of the data contained in the figures.

We believe that there is a vast information potential inherent in the global measurement of radiation by means of satellites and, if the reader of these pages comes away sharing that conviction—at least in part—this document will have amply served its purpose.

WILLIAM R. BANDEEN
Goddard Space Flight Center
Greenbelt, Maryland

Page intentionally left blank

CONTENTS

LIST OF FIGURES

A QUASI-GLOBAL PRESENTATION OF TIROS III RADIATION DATA

A quasi-global "synoptic" map of the radiation in the atmospheric "window" (8 to 12 microns) as derived from TIROS III, Channel 2 measurements is presented for July 16, 1961. This map, covering the globe between 55°N and 55°S, is superimposed on various conventional synoptic analyses to study the utility of the satellite radiation data for meteorological analysis purposes.

INTRODUCTION

The TIROS III meteorological satellite was equipped with a five-channel medium resolution radiometer to measure the reflected solar radiation as well as the infrared emission of the earth-atmosphere system in five different spectral regions (Reference 1). According to the initial design of this radiation experiment, one of the most useful applications of the infrared measurements was to be the derivation of day and nighttime cloudiness from Channel 2, which was sensitive within the atmospheric "window" region (8 to 12 microns). Several authors already have demonstrated and discussed the principal usefulness of these data for this particular purpose (References 2, 3, and 4).

This present study was performed to investigate and demonstrate the utility of the TIROS radiation data for global synoptic analyses.

July 16, 1961, was selected (Reference 5) for this study because it was a typical mid-season day and had a better-than-average radiation data coverage. Additionally, this particular day shows a number of most interesting synoptic features all over the globe, such as an intensive frontal system over the United States including a squall line, four tropical storms in the Atlantic and the Pacific Oceans, the well-developed Asiatic monsoon, and many others. Because of the observed instrumental degradation of the radiometer (Reference 6) it was most desirable to initiate a study during the early operational days of TIROS III, which was launched on July 12, 1961.

THE QUASI-GLOBAL RADIATION ANALYSIS FOR JULY 16, 1961

Orbital Pattern

Generally, the orbital inclination of 48 degrees limits the radiation and television data acquisition to latitudes 55°N to 55°S. Because of the specific locations of the two data readout stations at Wallops Island, Virginia, and Point Mugu, California, the number of readout orbital passes was limited to eight. As a result, wedge-shaped areas of an uninterrogated pass near 90°E (Northern Hemisphere) and 90°W (Southern Hemisphere) occur. In this case, the northbound portion of the TIROS III orbital passes occurred essentially in darkness while the southbound path of the satellite occurred in daylight. Hence the portion of the map lying east of the diagonal running from 20°S, 45°E to 20°N, 90°E consists largely of nighttime data, while the area west of this line consists of daylight recordings.

The subsatellite tracks of the seven selected readout orbital passes in this analysis are shown in Figure 1. Unfortunately, orbital pass 59 was not successfully acquired. The radiation map, shown in color as a basic part of Figures 1 through 6, was produced from non-overlapping data points of the selected orbital passes. Thus, orbital passes 56 to 60 were not permitted to cross later passes (at center of Figure 1).

The solid and dashed lines of the subsatellite tracks indicate the single and alternating open modes and closed modes, respectively. The beginning and end times of these scanning modes are shown in minutes with respect to the ascending node time.

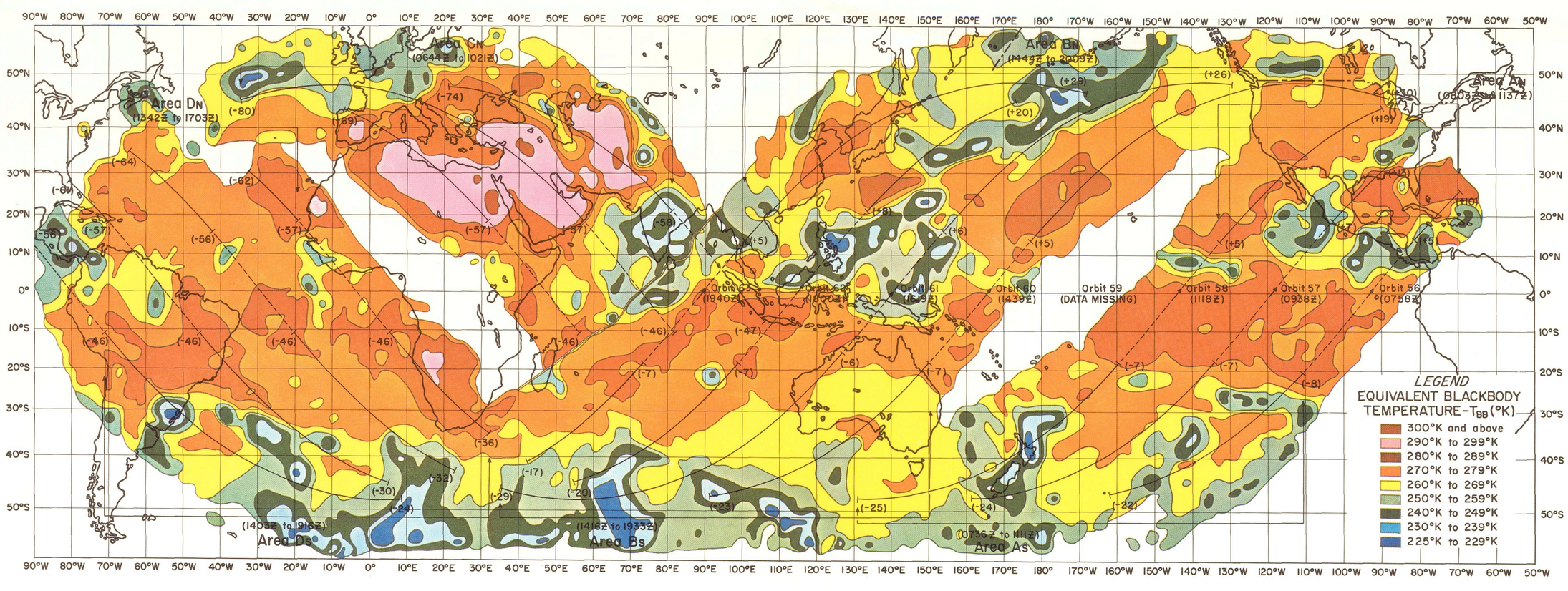

FIGURE 1. Pattern of the orbits of TIROS III used for the quasi-global radiation map (Figures 2, 3, 4, 5, and 6). The orbital numbers and the related ascending node times are drawn at the beginning of each orbit. The numbers along the orbital tracks are minutes from ascending node time.

Method of Analysis

The seven orbital passes were processed into grid print maps by an IBM 7090 computer using a resolution of 2.5 degrees longitude/mesh interval and a nadir angle limitation of 58 degrees. The isolines of Channel 2 equivalent blackbody temperature of T_{BB} were then drawn manually on the assembled maps. The data were not corrected for instrumental degradation, limb darkening, and mislocation within the areas of closed scanning mode. After each consecutive orbit was positioned on a world mercator chart (1:20 million scale), the overlapping infrared data boundaries were subjectively joined by the analyst.

The quasi-global surface synoptic analysis was adjusted by using all available weather central analyses and synoptic data to approximate orbital times, starting at 0600Z, July 16, 1961 (Reference 7–a to o), and drawn independently of the TIROS III radiation analysis (Figure 2). The 500 mb constant pressure chart (Figure 3) was derived essentially from the 0000 and 1200 GMT charts, and was unchanged from the source analyses (Reference 7–g, o). The 300 mb constant pressure chart (Figure 4), the vertical motion and vorticity chart (Figure 5), and the 200 mb streamline analyses (Figure 7) were drawn from several sources for 1200 GMT (Reference 7–g, o). The latter analysis is essentially the contribution of Lt. Col. James C. Sadler, USAF, Institute of Geophysics, University of Hawaii. Finally, a revised surface weather analysis was added (Figure 6), which used the radiation information directly for assistance in the surface analysis over certain geographical areas.

Synoptic Weather Discussion

The purpose of presenting this set of quasi-synoptic maps (Figures 2 to 7) in combination with the distribution of Channel 2 equivalent blackbody temperatures is to demonstrate the degree of correspondence between the radiation patterns and the different weather systems derived from conventional data.

Regardless of limitations imposed on the TIROS radiation data by the design factors of the satellite radiometer and by the data processing system, cloudiness is the primary factor which determines the distribution of equivalent blackbody temperatures in the analyzed charts. In a broad sense, the average distribution of temperature with height may be considered uniform enough in the zone bounded by 40°N and 20°S (desert areas excepted) in July so that a single high inverse correlation between equivalent blackbody temperature and the elevation of cloud tops can be assumed provided opaque overcast clouds exist. South of 20°S for this July case, in the winter hemisphere, a latitudinal change toward lower temperatures for given heights of cloud tops can be assumed, since vertical temperature gradients decrease zonally to the south. In the Northern Hemisphere, both continentality and latitude must be considered to obtain the heights of cloud tops north of 40°N.

The isolines of equivalent blackbody temperatures (Figure 2) show all the well-known synoptic features of the atmospheric general circulation in July. The polar fronts, represented by the long chains of high, "cold" (225° to 260°K) cloud systems, are in their northernmost location in their respective hemispheres, distinctively separated from the tropical convergence zones by well-pronounced belts of warm radiation temperatures (270° to 290°K) in the cloudless or less cloudy subtropical high-pressure regions.

The Northern Hemisphere is close to its annual heat maximum in July. Several cloud-free desert areas in North Africa and the Near East show maximum equivalent blackbody temperatures as high as 310°K. These and other deserts, as well as semiarid or summer-dry climatic regions of the Northern Hemisphere, are clearly outlined by 280° to 290°K isolines. In interpreting the maps, one must keep in mind the effect of slight limb darkening as the nadir angle increases toward 58 degrees near the data area boundaries.

The separation of the Sahara from the Saudi Arabian Desert and the break between Saudi Arabia and the Iran–Afghanistan–Turkmen region show up well, with slight mislocation. The 290°K isoline follows the Mediterranean coastline, separating the hot arid desert from the cooler sea region. The warm plateau of Turkey, the Iberian Peninsula, and the desert areas of southwestern United States are pronounced in a similar pattern.

The intertropical convergence zone is well characterized by the low radiation temperatures (230° to 260°K) of its high-reaching cloud systems and can be traced nearly around the globe.

The widespread southwest monsoonal cloud system shows up very distinctly over India, the Indian Ocean, and Southeast Asia. Tropical storms Flossie, Kathleen, and Liza are clearly shown by "cold" T_{BB} values close to the Philippines and to the southwest coast of Mexico, respectively. The early stage of Hurricane Anna is shown by the singular cloud system at 10°N, 40°W. The slight elongation is an erroneous distortion caused by misplacement of data in the closed scanning mode.

On this day, over the Southern Hemisphere, as would be expected, the winter season storms reach to far lower latitudes than do the summer season storms over the Northern Hemisphere. The extensive frontal systems, in all stages of development, are shown even north of 20°S over South America, close to the tip of South Africa, and along 20°S, in the vicinity of Australia. The subtropical high-pressure belt is also shifted northward, and its high T_{BB} values (270° to 290°K) reach nearly around the globe. A most noticeable hot area (300°K) is in Southwest Africa, northwest of the Kalahari Desert.

The upper air maps (Figures 3, 4, and 7) support the general synoptic picture described above. The major frontal zones coincide with the large extratropical cloud masses, as indicated by the lower radiation temperatures, while the tropical cloud masses are accompanied by weak mid-trophospheric pressure gradients and easterly flow at the 300 and 200 mb levels.

A very important comparison is that between the radiation field and the vertical motion and vorticity pattern shown in Figure 5. The maps of these dynamic properties were taken from the routine maps produced daily by the Numerical Weather Prediction Unit (NWP) at the National Meteorological Center (NMC) of the U.S. Weather Bureau, Washington, D.C. The vertical motion pattern determined by the divergence fields at 850 and 500 mb is valid approximately for the 650 mb level. Therefore, a good correlation with cloud patterns can be expected only for those systems produced by large-scale processes which are not restricted to the surface boundary layer or by vertical motion processes in the upper troposphere alone. However, even with consideration of these restrictions, the correspondence between the computer vertical motion field and the large-scale cloud systems as derived from TIROS radiation measurements (Channel 2) is generally a very poor one with regard to any detail. This poor relation may be explained by the lack of conventional data over a large portion of the area and incomplete knowledge of the dynamical and thermodynamical factors associated with the development, maintenance, and dissolution of clouds.

A relatively good agreement between both fields occurs over the Northeast Atlantic, where the high-reaching cloud mass matches generally a pronounced area of upward motion. Another area of still better correspondence appears over the North Pacific polar front between the sea regions east of Japan and the Aleutian chain,

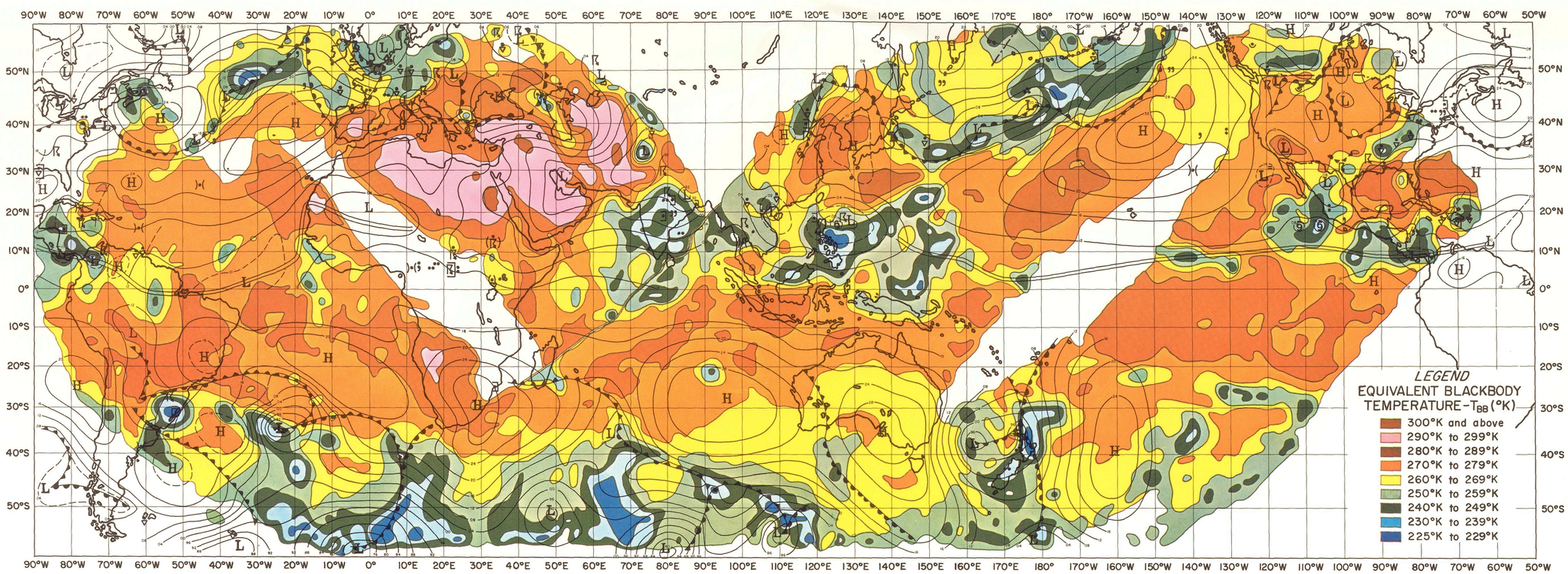

FIGURE 2. Composite map of "window" radiation (Channel 2) and surface synoptic analyses combined from different sources (Reference 7).

Page intentionally left blank

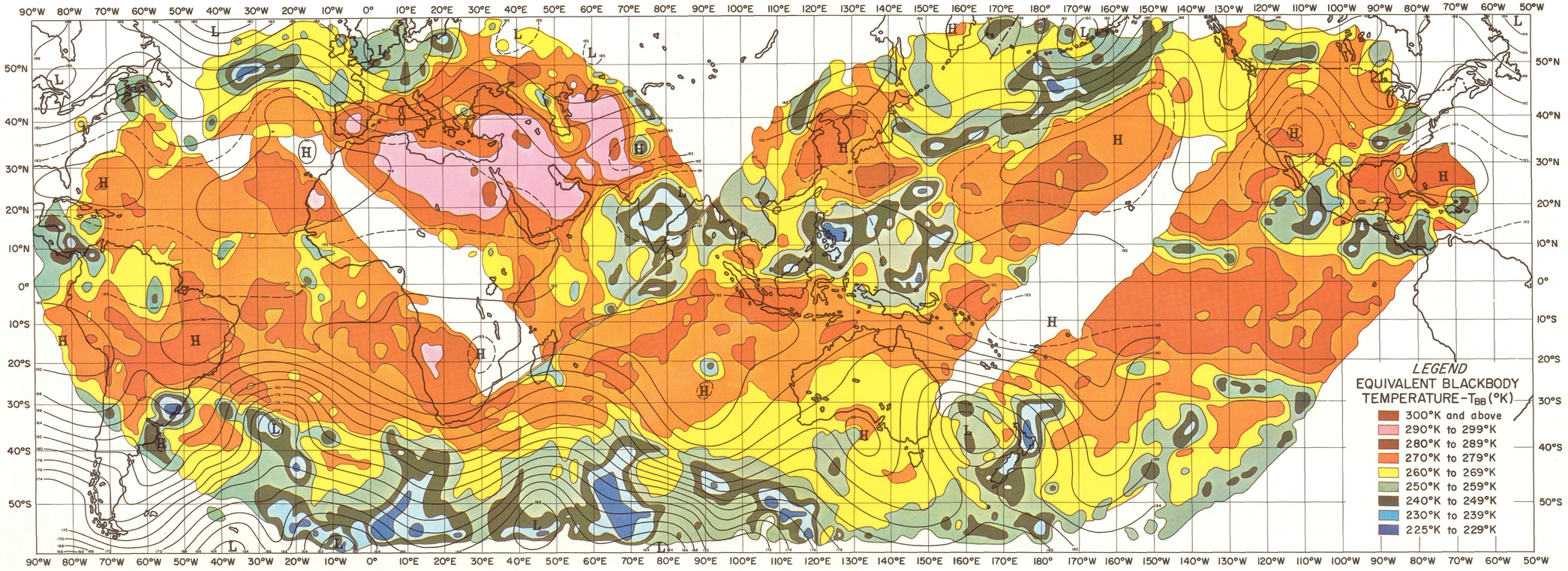

FIGURE 3. Composite map of "window" radiation (Channel 2) and 500 mb contours (hundreds of feet) combined from different sources (Reference 7).

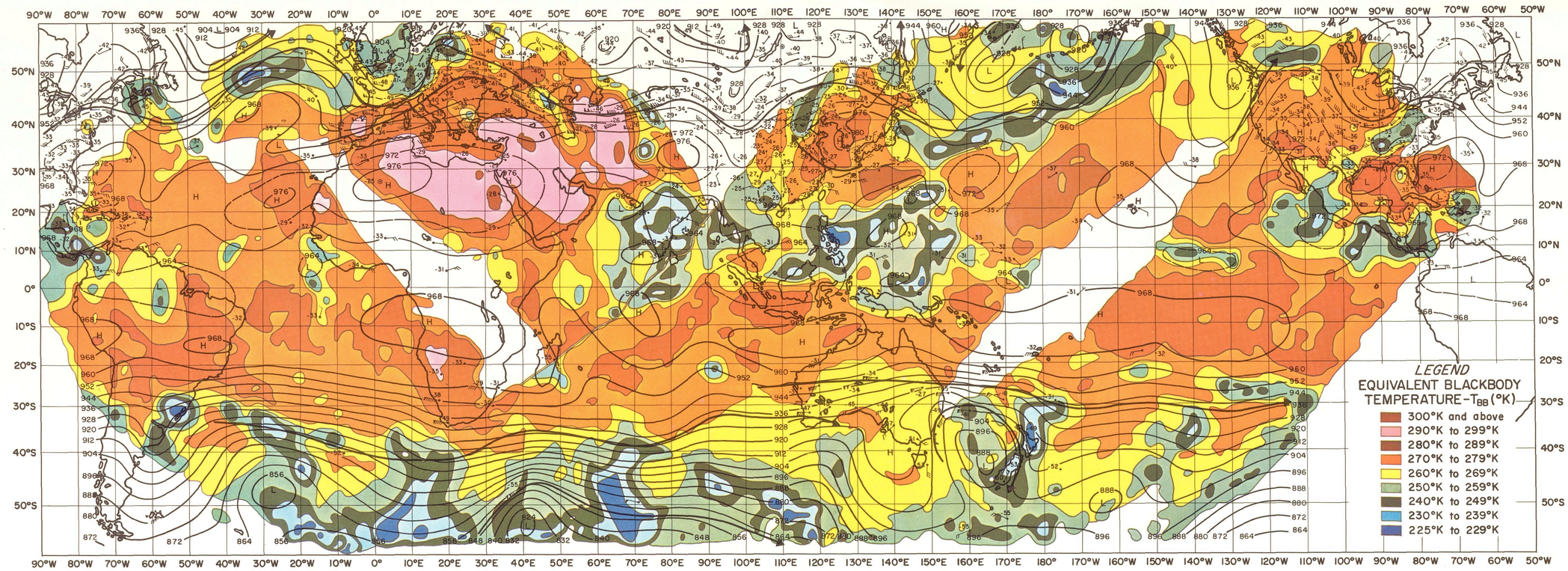

FIGURE 4. Composite map of "window" radiation (Channel 2) and 300 mb contours (decimeters) including the jet-stream axes (Reference 7).

Page intentionally left blank

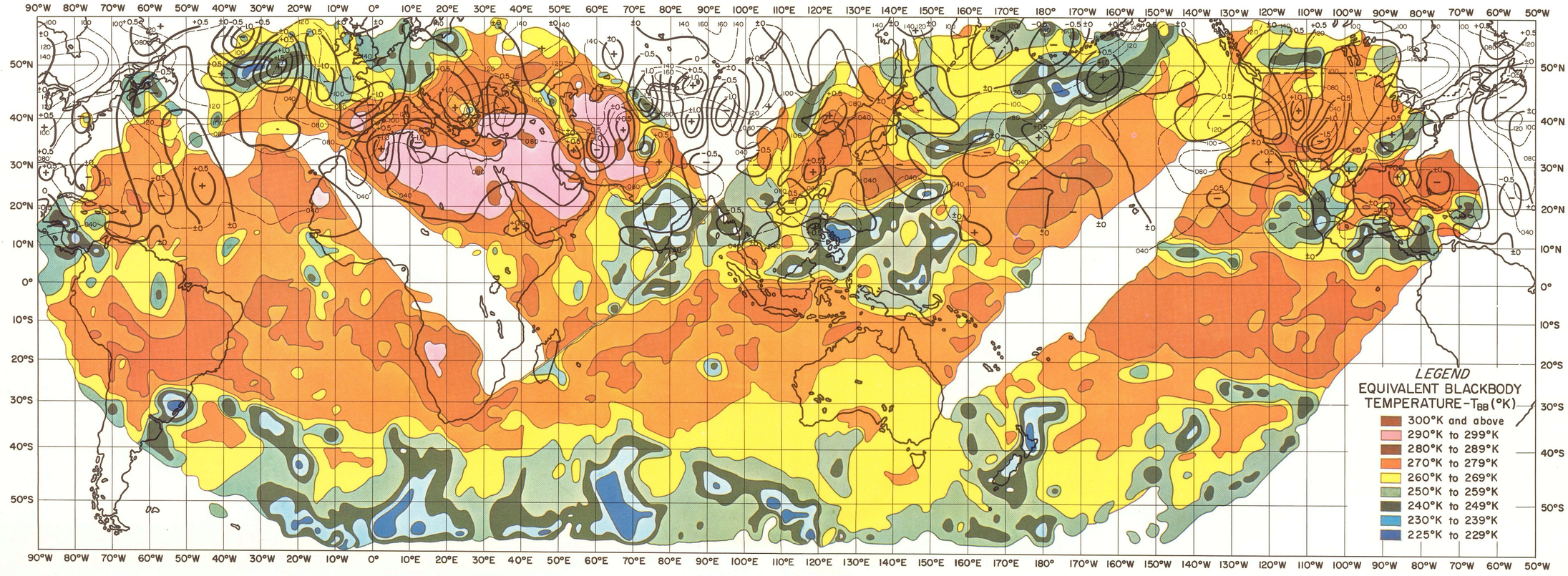

FIGURE 5. Composite map of "window" radiation (Channel 2) and vertical motion in cm/sec (solid lines; plus sign indicates upward motion) and absolute vorticity in 10^{-4}/sec (dashed lines).

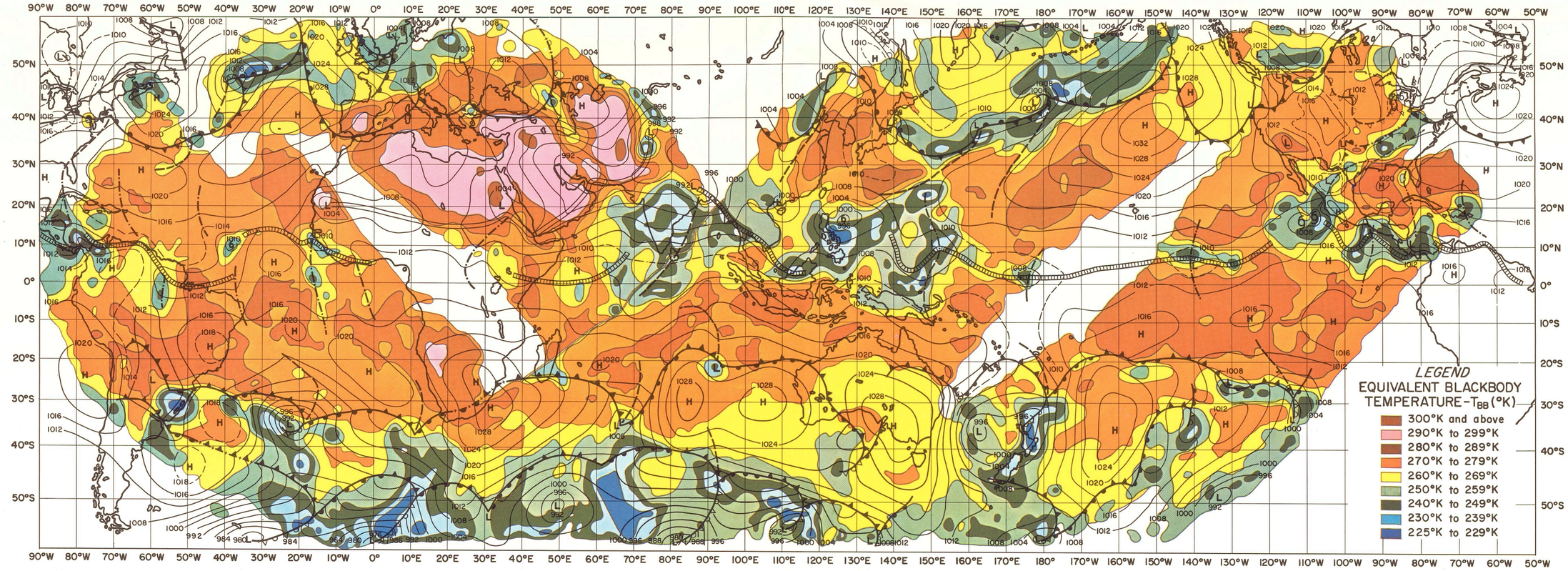

FIGURE 6. Surface analysis revised on the basis of TIROS III, Channel 2 radiation data.

Page intentionally left blank

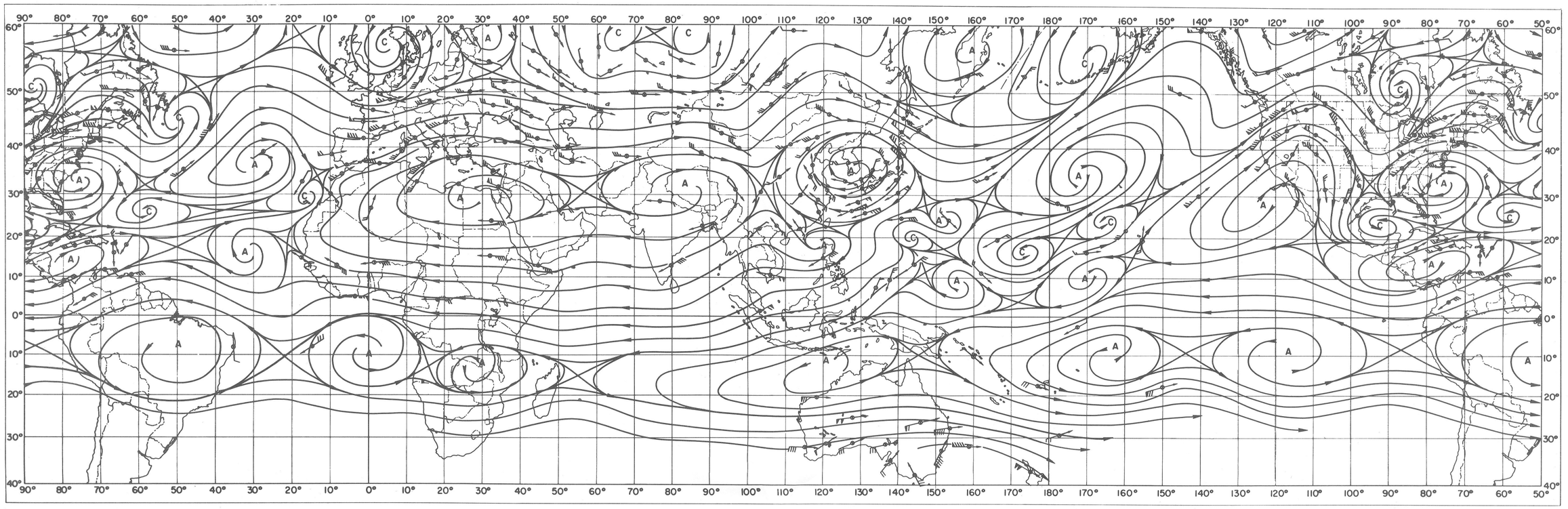

FIGURE 7. 200 mb streamline analysis, July 16, 1961; 1200 GMT.

where a continuous band of upward motion parallels the long frontal zone. The frontal system over the southeastern United States also is shown nicely in both the radiation and the vertical motion field, and one little cold spot over Bulgaria partially matches an upward motion center. The large monsoonal areas over Southeast Asia are mostly shown up as subsidence, while over Central India a very slight upward motion shows some relation to the monsoon clouds. However, because of the poor definition of the flow pattern in this area one cannot expect agreement here, as the NMC model depends highly on an exact knowledge of the flow pattern.

In all other regions, however, the structure of both fields seems different; and it is probable that either or both of the following conditions exist: (1) the vertical motion is derived from an inexact computer-processed atmospheric model, and (2) cloud fields are not uniquely defined by the upward vertical velocity fields. A good correlation seems to exist only in those regions of well-developed extratropical frontal zones, where the dynamical processes producing the cloud systems penetrate the larger parts of the troposphere and where the basic data for the NMC maps are adequate.

By comparing the 500 mb absolute vorticity chart and the cloud distribution in Figure 5, no better relation can be found. The large frontal clouds over the southeastern United States and the North Pacific are found in areas of relatively strong vorticity gradient; but in other areas of similar gradients, such as over the Rocky Mountains and the Mediterranean Sea, similar cloud systems do not appear.

Re-Analysis of the Synoptic Surface Map Due to TIROS Radiation Data

Since the synoptic weather analysis which was compared with the Channel 2 radiation data in Figure 2 was based on conventional data only, a complete agreement with the real conditions could not be expected in those areas where the missing observations forced the analyst to make rough extrapolations and subjective assumptions. Thus, although in general the depicted analyses and the chart of cloudiness derived from equivalent blackbody temperature show a surprisingly good relation, in many areas of sparse conventional meteorological data the radiation chart, interpreted as cloudiness information, suggested several changes of the surface analysis to bring it into better accord with the Channel 2 radiation field. Especially over the Southern Hemisphere, with its vast oceanic areas largely void of any conventional weather information, a reasonable and appropriate interpretation of the TIROS radiation information should lead to a considerably truer picture of the real atmosphere. The re-analyzed surface chart is reproduced in Figure 6. Some of the more significant changes applied to Figure 2 will be discussed in the next paragraphs.

In the North Pacific, the analysis was adjusted (Figure 6) along the frontal zone between Japan and the Gulf of Alaska to bring the high cloudiness (low T_{BB}) more in line with acceptable frontal models. In particular, the open wave near 45°N, 175°E has been changed to an occluded system, since a clear tongue in the high clouds indicated by warmer T_{BB} values intrudes from the west and northwest into the sea-level low-pressure center. This inferred cloudiness condition, depicted by the shape and distribution of the yellow, green, and blue colored areas (225° to 260°K) near the system fits the classical Bergeron model for cold-type occlusions (Reference 8). Boucher and Newcomb (Reference 9), Serebreny et al. (Reference 10), and Merritt (Reference 11) have made interpretations of extratropical cyclone patterns, as seen by TIROS television camera systems, which support the cloud system model associated with an occluded frontal system.

An interesting feature occurring within several warm sectors of frontal cyclones is the appearance of a cloudy zone beginning near the point of occlusion and extending equatorward, not directly related to the polar fronts. These zones are associated with cyclonic vorticity advection within the warm portions of lower tropospheric troughs, as may be seen by comparing Figures 3 and 5 over Mexico, Texas, China, and over the Atlantic at 30°N, 55°W. The instability zone over the United States developed into a squall line; and the zone in the western North Pacific case is well reflected in sea-level pressure and wind data. Even in vertical cross sections, these instability zones appear (as the discussion of Figure 17 will show).

Although the data presented in Figure 6 are for a single day only, it must be noted that both a summer condition (Northern Hemisphere) and a winter condition (Southern Hemisphere) are represented. Further, the aforementioned cloudy zones exist in both hemispheres with the more active extratropical cyclones. Thus, it is probable that such patterns are not simply seasonal but are a definite part of the total circulation state. The variations of intensity of weather activity along any one of the zones show a spectrum which may be equated, in a general sense, to the cloudiness intensity spectra postulated for different types and different degrees of intensity of the classical polar frontal conditions. Therefore, these zones suggest that the "induced trough" (Riehl, Reference 12), the "meridional front" (Palmer, Reference 13), and the "instability line" (Fulks, Reference 14) are closely related phenomena of the warm sector of polar front cyclones, differing only in respect to the intensity of cloudiness development. Note that the revised analysis (Figure 6) indicates these zones as dashed lines (commonly used for troughs), assuming that the phenomena are related to and should be a real part of the frontal model. (Note that over the United States the squall-line symbol was used, since the activity was very intense.) It may be worthwhile mentioning that even in the revised analysis these instability lines have been drawn only where real justification is given by conventional or radiation data. Therefore, in several more cases similar phenomena may exist over remote areas without a simple detectable response in the cloudiness pattern as derived from satellite information.

Three different types of lines are used in the tropical zones to characterize the basic circulation features in their actual positions on July 16, 1961. The easterly waves are symbolized by dash-dot lines. Two parallel lines are used to indicate the Intertropical Front (ITF), which is the boundary line between continental tropical and maritime tropical air masses. The near-continuous zone of tropical convergence (ITC) which exists wholly within maritime tropical air is symbolized by two parallel lines with crossing slashes. As the boundary between continental tropical (cT) and maritime tropical (mT) air masses in July over Africa and Southern Asia has an appreciable slope, with the mT air below being denser than the cT air aloft, the lower radiation temperatures which denote high cloudiness occur a considerable distance from the sea-level location of this zone (200 or more miles away, in the mT air). On the other hand, the condition analyzed by the second definition (ITC) is essentially arrayed vertically, and the high cloudiness zones are expected to be almost directly over the sea-level position of the convergence zone.

Page intentionally left blank

The analysis over West Africa, for example, is supported by two mosaics of television pictures taken on July 16 and 17, 1961 (Figures 8 and 9) in addition to the radiation pattern. The intertropical front, as defined above, is assumed somewhat north of the areas of cloudiness shown in the pictures, meeting the African west coast within the low, close to Cape Blanc, where in the radiation map the temperature begins to decrease southward. Along the coast of the Gulf of Guinea a pronounced zone of heavy cloudiness, shown as a yellow and green area in Figure 6, may be considered perhaps as the maritime type of the tropical convergence connected with the ITC over the Atlantic. It is difficult in this case to distinguish between a real ITC and a merely coastal effect; but Figure 8 shows that near 5°N the cloud mass, definitely diverging from the coast line, supports the assumption that there is a large-scale dynamic formation of this cloudy convergence zone. The analysis of two easterly waves or at least meridionally oriented convergence zones is based on the two zones of considerably lower radiation temperatures extending southward from the Guinea coast. The one located more easterly is weakly shown in the radiation field but is supported by the broken cloud system at the right lower fringe of the mosaic in Figure 9.

In Figure 6 the African tropical front has been extended into the Indian monsoon low, separating again the continental and maritime air masses. Also, the radiation pattern seems to

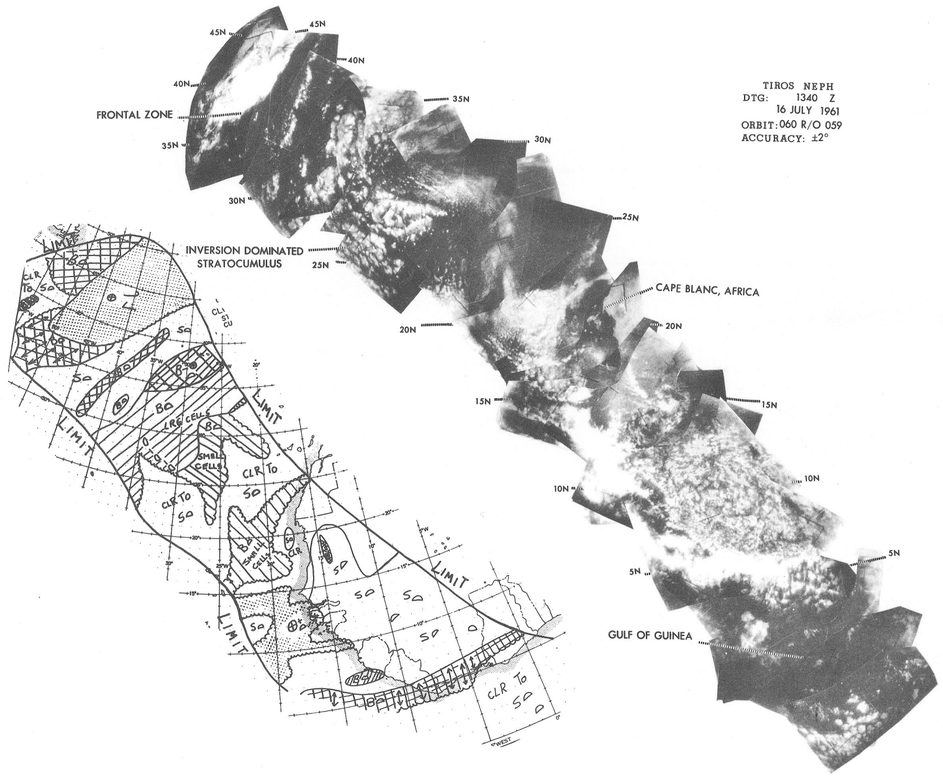

FIGURE 8. Mosaic of TIROS III television pictures over West Africa and the adjacent Atlantic Ocean on July 16, 1961.

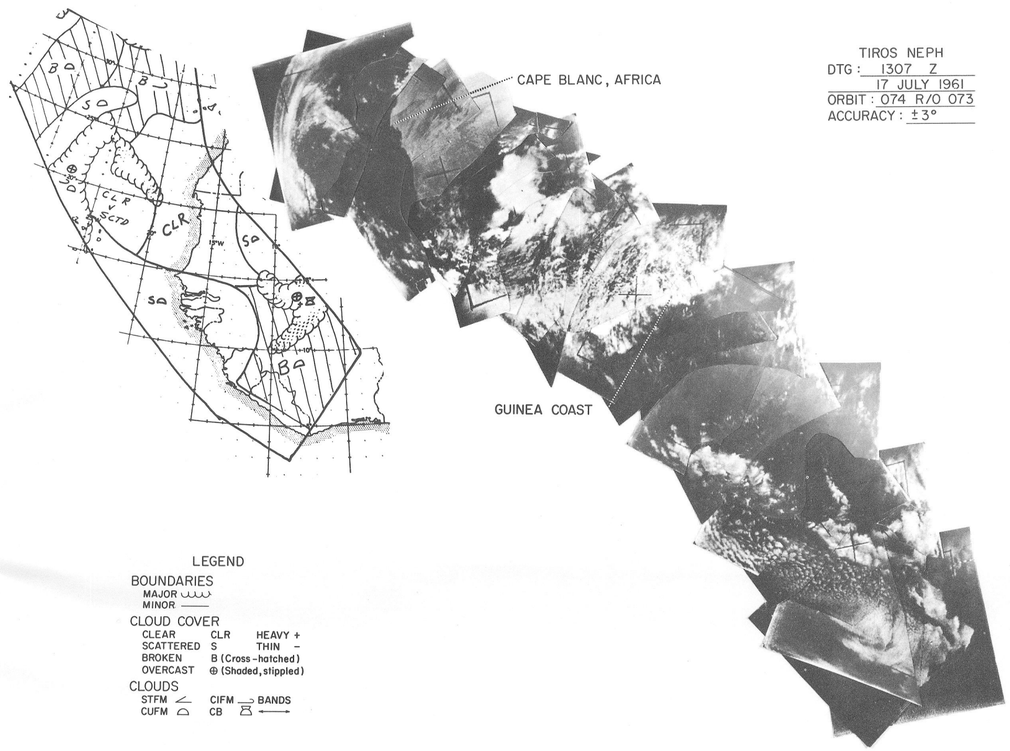

FIGURE 9. Mosaic of TIROS III television pictures over West Africa and the adjacent Atlantic Ocean on July 17, 1961.

show the existence of a convergence zone close to the equator off the East African coast. This intertropical convergence zone (ITC) is visible in the TV mosaic as a banded cloud system, whereas the larger cloud system toward the southeast has been assumed to be associated with the line of convergence extending southward from the Bay of Bengal.

A special point of interest is the structure of the Indian monsoon cloud system shown in the TIROS radiation data. The Channel 2 radiation chart of Figure 10(a), presented in more detail (1:10 million scale) than in the large world colored charts, shows the very complex picture of the monsoonal cloud systems supported by the Channel 5 "visible" chart (0.55–0.75μ) in Figure 10(b). In these patterns the meridional zone of opaque and high-reaching clouds south of India seems to exist and has been analyzed as a line of significant organized convergence. Along the coast of Burma another banded structure is apparent, interpreted as a part of the ITC in Figure 6. Several isolated higher cloud systems are detected over the Bay of Bengal within an extensive cloud shield of the Indian subcontinental region. However, a relative maximum over central India may suggest lower cloud tops.

At the apex of the Indian subcontinental plains and an arch of the Himalayas, a monsoonal low center is marked by a pronounced high-reaching cloud mass. Although this center is indicated as the eastern terminus of the intertropical front, this cloudiness is not considered characteristic of the ITF. Rather, a strong orographic effect is the more probable cause.

Page intentionally left blank

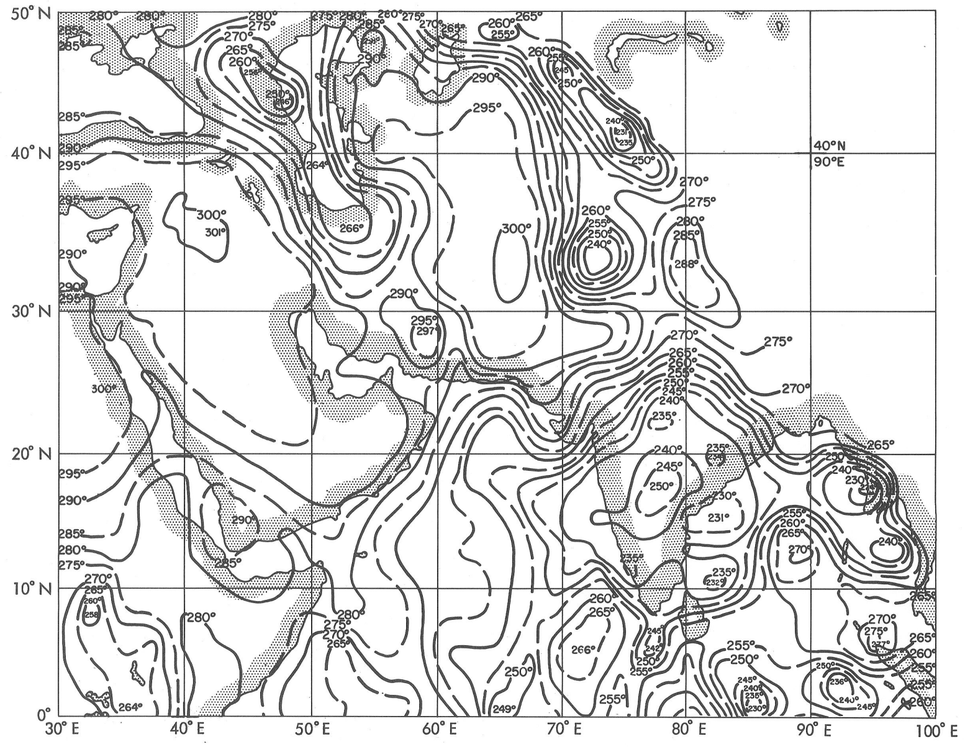

(a)

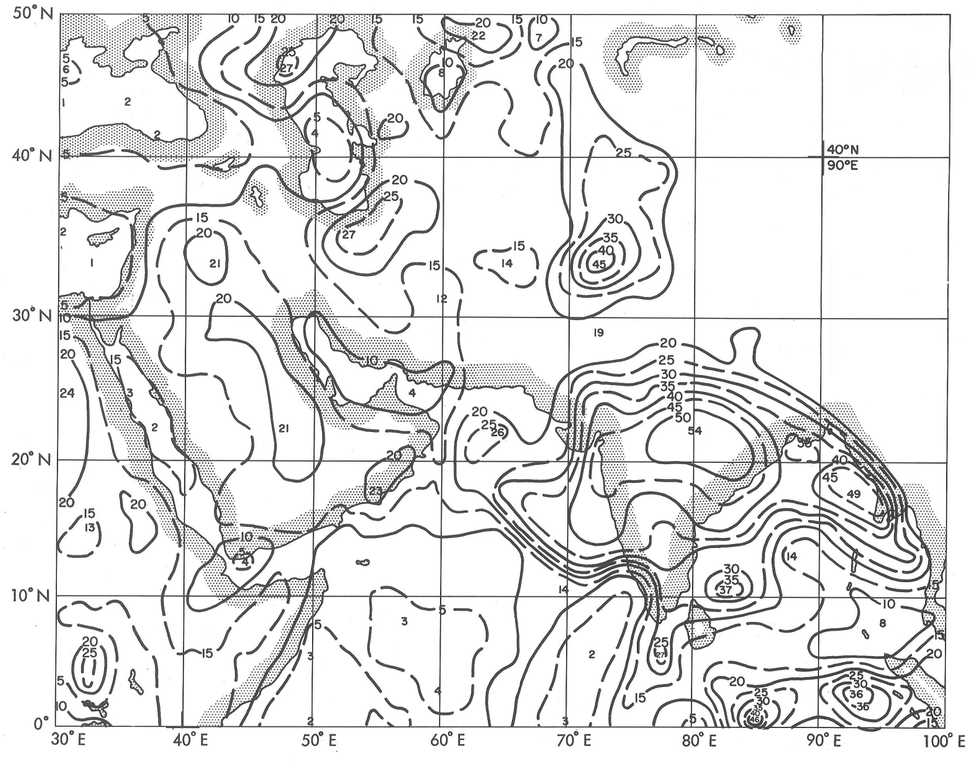

(b)

(a) Channel 2 "window" radiation (T_{BB}; °K)
(b) Channel 5 reflected visible radiation (w/m²)

FIGURE 10. Radiation analyses of two TIROS III channels on July 16, 1961, over the Near East and India.

About 2 degrees southwest of this center and thence to the western limit of the ITF, the analysis shows this front to exist as a cloudless zone, which is in agreement with the model given by Sawyer (Reference 15). Figure 11 gives Sawyer's schematic cross section through the intertropical front over Pakistan, where the dry continental air (*cT*) overrides the moist denser monsoon air (*mT*) at the frontal surface. In the clear areas of the *cT* regime the sensitivity of the radiometer is well demonstrated. The fact that the Red Sea and the Persian Gulf are cooler than the desert areas close to local noon is well pronounced in the Channel 2 radiation maps, whereas the Channel 5 data detect a very small amount of reflected solar radiation from these darker sea regions and higher values over the brighter deserts. A small relative misalignment between Channels 5 and 2 could even be inferred from the slight displacement of the lower values in these areas.

Over the Indian Ocean, near 20°S and 90°E, the satellite radiometer locates an area of high extended cloudiness which does not meet the concept of a large anti-cyclone as indicated by the original analysis (Figure 2), but rather suggests the cloudiness state of a small cyclone (Figure 6). For this reason a small wave cyclone was assumed in the re-analysis on the weak front between Australia and the low near 35°S, 65°E. This fits very well the vortex shape of the bright cloud mass in the bottom section of the television mosaic presented in Figure 12. Additionally, the appearance of a cyclone in Western Australia three days later could be better explained by the continuity of this newly developing wave.

Distinct bands of cloudiness in the South Atlantic and South Pacific Oceans strongly suggest a double frontal model, but the South Indian Ocean radiation data are not easily split into two zones. However, in light of the conditions over the Southern Hemisphere oceans and a suggested existence of two major jet-stream axes within the conventional data located in or near the Indian Ocean and the Southern Pacific Ocean, the revised analysis depicts a double frontal model throughout the Southern Hemisphere. In addition, the analysis has been extended into the central South Pacific, a region which had not been analyzed by any of the Southern Hemisphere weather centrals because of a complete lack of data. Naturally, the extension based on radiation data alone can be only a probable solution combining both the suggested cloudiness information derived from TIROS III radiation data and the conventional long-wave frontal models.

In general, the location of high cloudiness and the jet-stream axes fits the conclusions of various investigators [Riehl (Reference 16), Serebreny et al. (Reference 10), Merritt (Reference 11), etc.]. We must note, however, that the jet-stream analysis, shown on the 300 mb chart (Figure 4) is a solution, based on conventional data, which has not been altered to fit the radiation pattern.

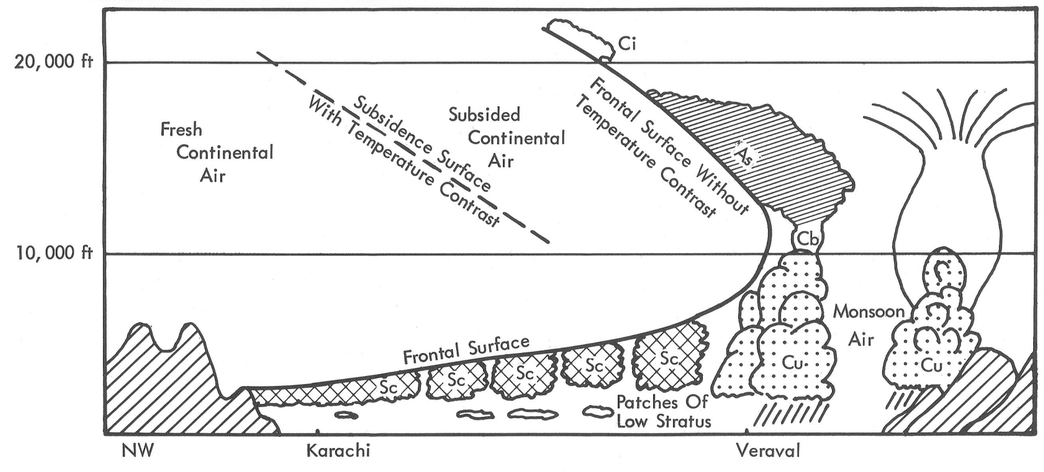

FIGURE 11. Schematic cross section through the intertropical front over Pakistan (after Sawyer, Reference 15).

Page intentionally left blank

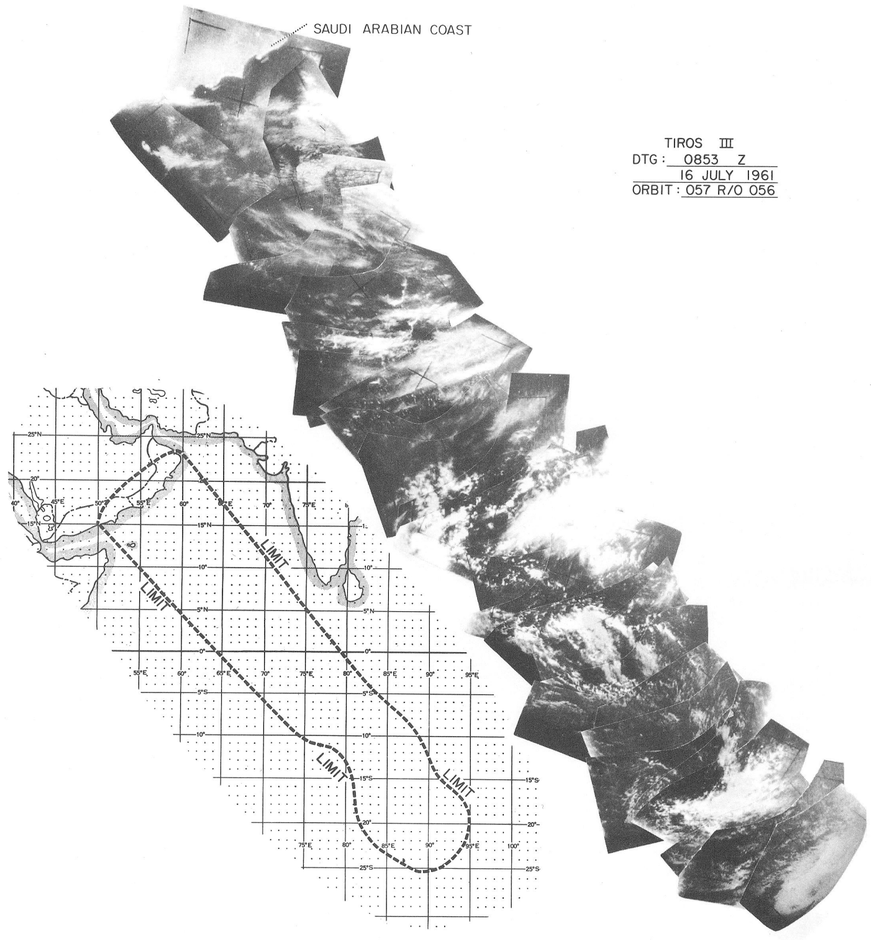

TIROS III
DTG : 0853 Z
16 JULY 1961
ORBIT : 057 R/O 056

FIGURE 12. Mosaic of TIROS III television pictures over the Indian Ocean on July 16, 1961.

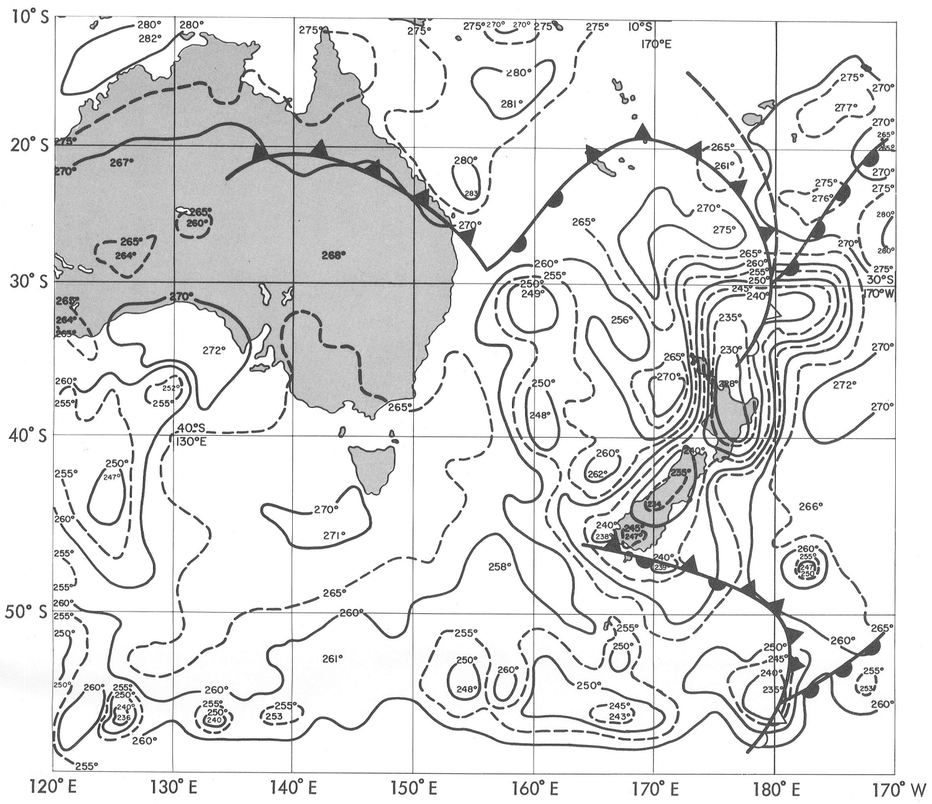

FIGURE 13. Channel 2 radiation analysis (T_{BB}; °K) and final frontal analysis on July 16, 1961, over Australia and New Zealand (orbital pass 57).

In the area east of Australia, the correlation between the initial surface analysis (Figure 2) and the radiation pattern apparently was not good. Thus, several changes have been suggested with regard to the new information provided by the satellite radiation data. In Figure 13 a more detailed analysis of the Channel 2 radiation field, based on a 1:10 million computer grid print map, is reproduced with the new frontal positions within the large cyclonic vortex over the Tasman Sea. The TIROS data indicate the highest dense clouds over New Zealand and somewhat north of it. The cold areas over South Island, New Zealand, may be interpreted as being produced primarily by orographical effects which are in accordance with the climatological average zone of high cloudiness presented for July by Haurwitz and Austin (Reference 17). Therefore, it seems appropriate to expect the point of occlusion to be close to this area at about 30°S. The occlusion of this old vortex with a cold core (Figure 3) encircles the vortex center rather than meeting it as is done in Figure 2. The cold T_{BB} areas around the South Cape of New Zealand appear to belong to another cyclone which is located farther south at the boundary of the map. The "cold" area at its point of occlusion may, however, not be limited to the south as indicated at the fringe of the radiation pattern.

The original analysis over the southern North Atlantic did not indicate any cyclonic activity near 10°N, 40°W; but the re-analysis has been made to fit the perturbation indicated by both satellite radiation data and television pictures. Fritz (Reference 18) showed that Hurricane Anna developed from a low-pressure area originally located over Africa. He used satellite pictures and conventional data to justify the location of Anna near 10°N, 39°W on July 16, 1961. The radiation data of TIROS III also justify the indicated location of the early tropical storm stage of this hurricane (see colored maps).

Page intentionally left blank

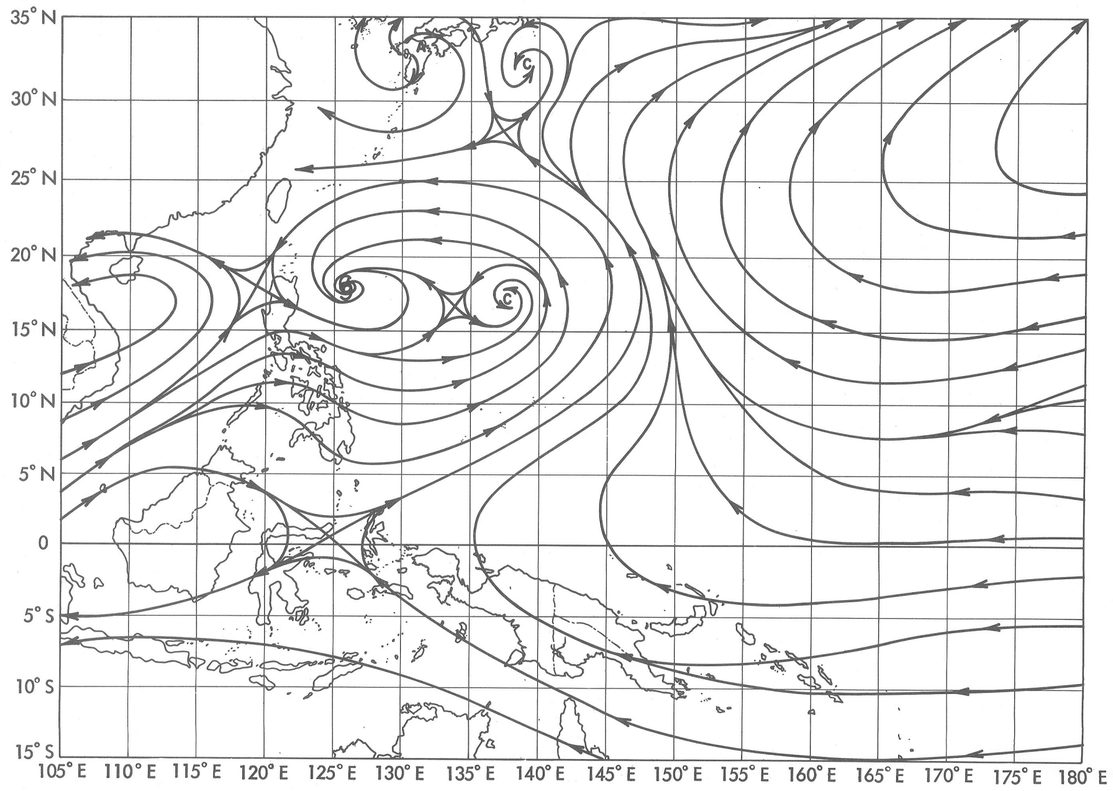

FIGURE 14. Surface streamline analysis on July 16, 1961, over the Western Pacific Ocean.

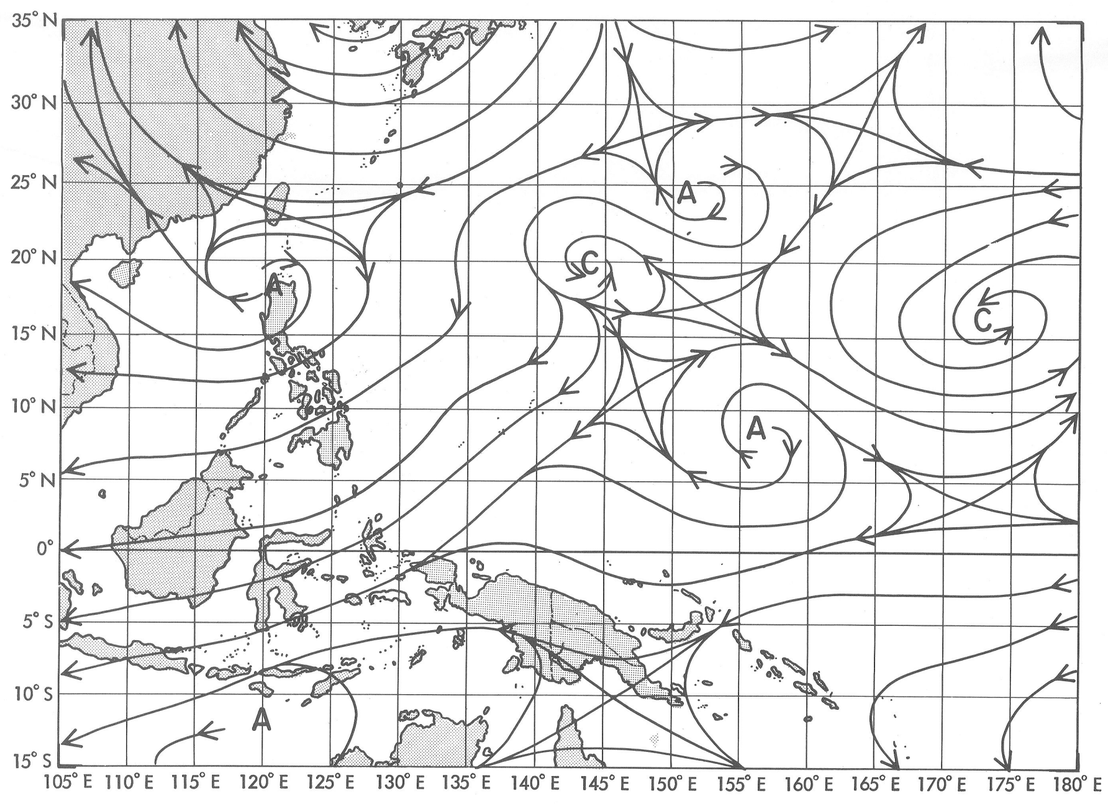

FIGURE 15. 200 mb streamline analysis on July 16, 1961, over the Western Pacific Ocean.

For the western North Pacific, where Tropical Storm Flossie occurred on the radiation map, some special maps are presented (Figures 14 to 18). The surface streamline analysis (Figure 14) shows Flossie east of Luzon and a tropical depression northwest of Guam (17°N, 138°E). At 200 mb (Figure 15) Flossie shows a slightly anticyclonic flow, a strong easterly jet stream being located just south of Japan (see Figure 4). A detailed picture of cloudiness is shown by TIROS radiation data (Figure 16), which was hand plotted from computer listings. Minimum equivalent blackbody temperature of 200°K indicates that heavy cloud masses extend up to the tropical tropopause, at least to 15 km height, if one considers the actual vertical temperature distributions surrounding the storm area (Figure 17). This radiation map (Figure 16) even gives some indications of the spiral structure of the tropical storm, the larger part of the cloud mass apparently being on the south side of the storm center, which is marked by the common tropical storm symbol. Figure 18, which is based on a 1:20 million computer grid print map for the Western Pacific Ocean indicates only those parts of the cloud mass where the radiation temperature in Channel 2 is above a system-designed threshold value (Reference 1).

For the western North Pacific a vertical cross section (Figure 17) along 140°E was drawn, based on conventional radiosonde data (Reference 7–o). The temperature distribution suggested the placement of the Japanese cold front at approximately 35°N, in good agreement with the indicated jet-stream core. The upper limit of the cold dome behind that front is shown by the frontal surface which is strongly inclined to the north. A dip in the generally horizontal isotherms between 20°N and 25°N, mainly based on the sounding at Iwo Jima, is assumed to be the justification for the instability line analyzed in Figure 6. The sudden dip of the isotherms caused an appreciable vertical instability between 3 and 7.5 km. Thus, the cross section gives a good idea of the vertical extension and structure of this perturbation. North of the line we find the warmest driest air at this longitude indicating strong subsidence; whereas, on its southern side, heavy cloud systems are rising to high altitudes as indicated by the radiation measurements of the satellite (Figure 18). Although there are no cloud reports by ships on this day at that longitude between 15°N and 25°N, the Japanese Weather Maps (Reference 7–h) of the preceding and following days give more information on the heavy mass of dense altostratus as well as strong cumulus development and shower activity in the whole area.

Thus, the analysis of cloudiness (dark shading in Figure 17) from 5°N to 25°N has been fitted, subjectively, to the heavy line of the reported Channel 2 radiation temperatures since prior and subsequent cloud observations support such a widespread cloud mass of cirrostratus, altostratus, and cumulonimbus (Cs, As, and Cb) elements. Additional analyses of cross sections in other areas (not included herein) support, generally, this relation of cloud tops to the reported radiation temperature when the cloud mass is opaque and predominantly overcast. These investigations show the temperature at the top of a deep dense cloud mass as conventionally determined from radiosondes to be nearly equal to that derived from TIROS radiometer, Channel 2 data. However, in the cases of scattered cloud areas and transparent cloud decks, the cloud heights cannot be interpreted uniquely from the satellite data. Different levels within the field of view of the radiation sensor and within the area of data averaging contribute to the detected radiation intensity and indicate a fictitious "effective radiation level" somewhere between all contributing levels (Reference 1). In these cases, the curve of radiation level does not match any observed cloud system as, for example, north of 38°N in Figure 17. To determine cloudy areas from radiosonde moisture information, one should consider the inaccuracies of the humidity elements at high relative humidities and at high altitudes, the instrumental time lag, the physical properties of clouds, etc. In this particular case, temperature–dew point differences of less than 2° to 3°C have been considered as clouds in the middle troposphere, while values of 5° to 8°C or even higher may be applicable in this sense in the upper troposphere, especially in the case of ice clouds. Thus, the moist layer at 300 mb between Sapporo and Alexsandrovsk probably represents an unreported (nighttime) cirrus which depressed the composite radiation temperature corresponding to the ambient air temperature above the altocumulus level of the lower cold dome at the frontal surface.

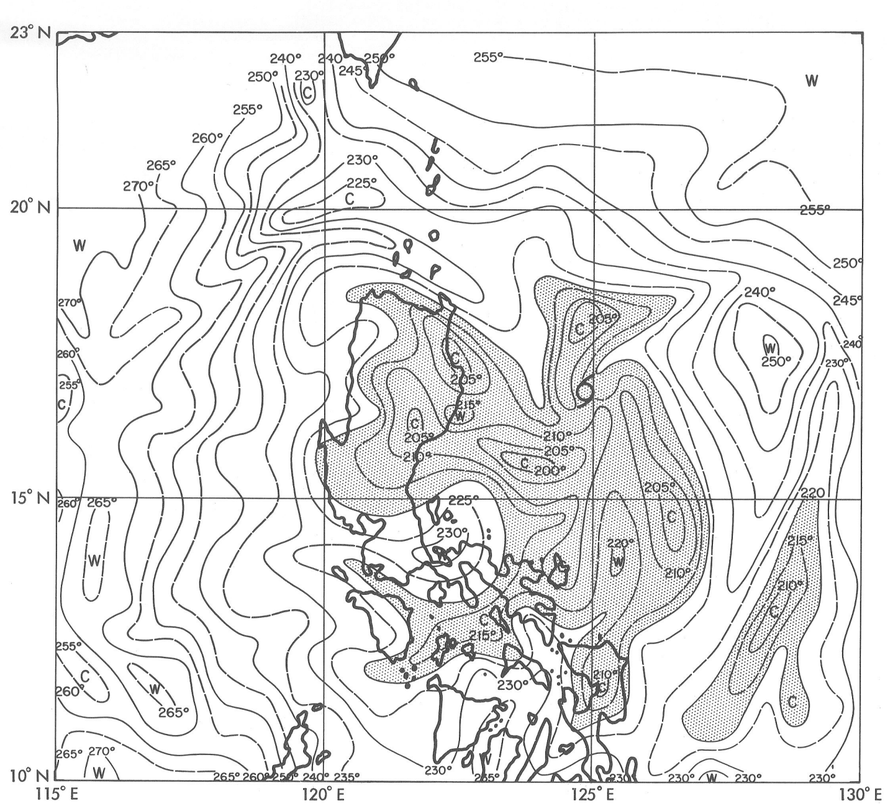

FIGURE 16. Channel 2 radiation analysis (T_{BB}; °K) over a tropical disturbance close to the Philippines. The shaded area indicates T_{BB} values below the threshold level. The storm center is marked by the conventional symbol.

Page intentionally left blank

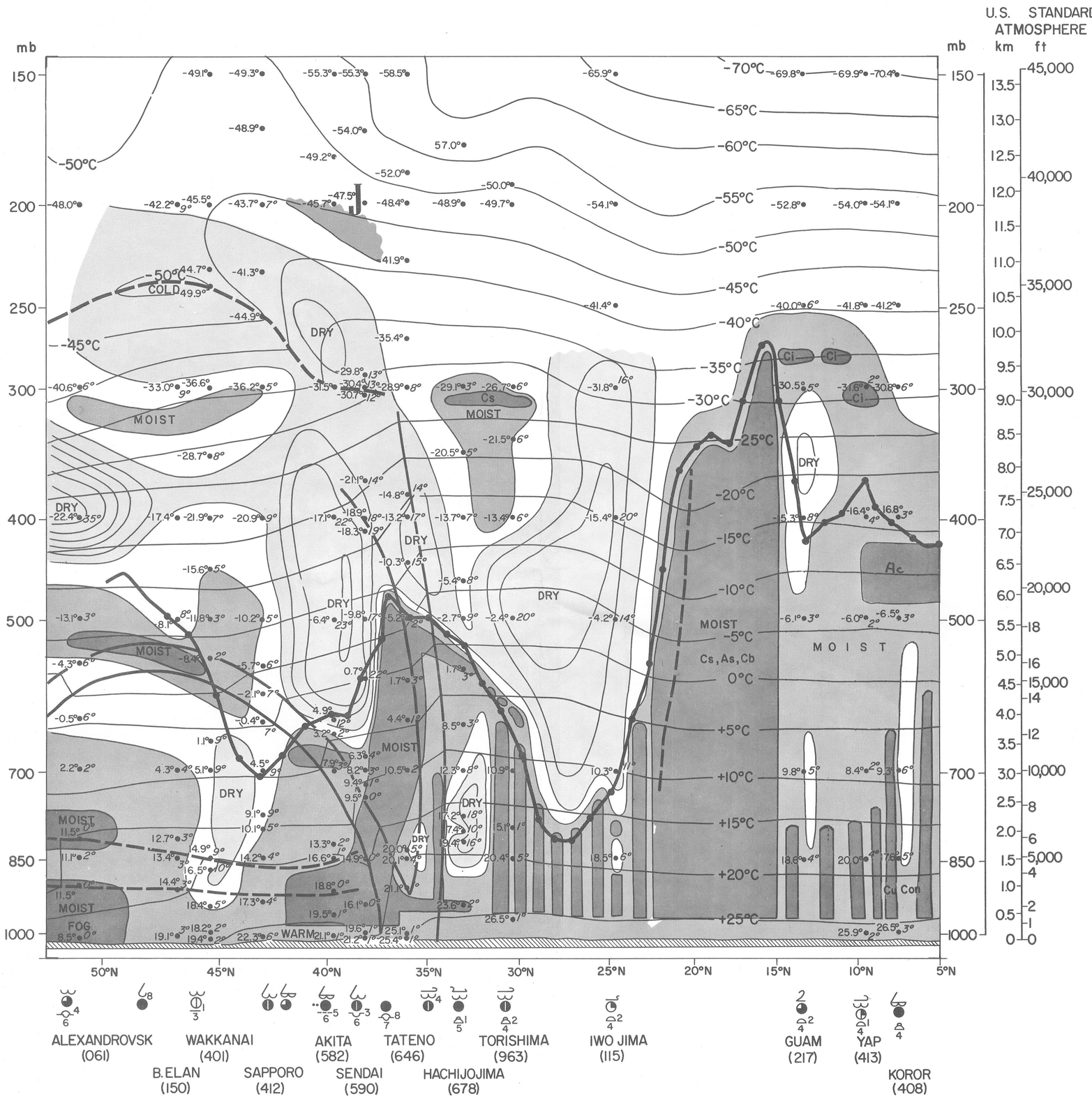

FIGURE 17. Vertical cross section along 140°E on July 16, 1961 (1200 GMT). Temperatures are in °C. Thermal discontinuities are indicated in a conventional manner. The humidity distribution is for practical reasons presented by isolines of temperature dew point differences in °C. Gray shades differentiate the significant moisture zones (light gray: more than 10° difference; medium gray: less than 5° temperature–dew point difference; dark gray indicates schematically cloud systems inferred by conventional and by satellite data). The heavy solid line with dots superimposed represents the "effective radiating heights" derived from equivalent blackbody temperature measurements of Channel 2, TIROS III. The jet-stream core is indicated by "J."

Page intentionally left blank

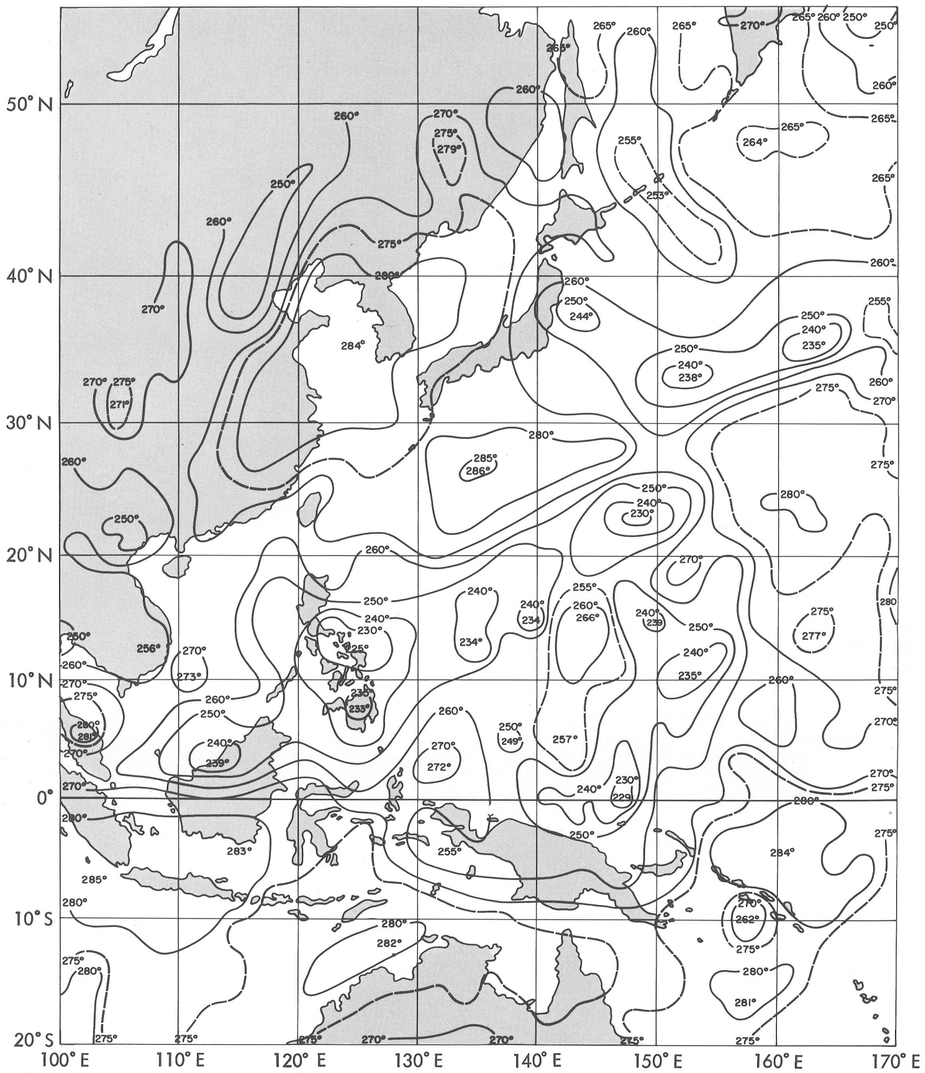

FIGURE 18. Channel 2 radiation analysis (T_{BB}; °K) for the Western Pacific Ocean on July 16, 1961.

CONCLUSION

Since the TIROS satellite is a spin-stabilized vehicle having fixed space-oriented cameras, only a restricted daylight portion of each orbit may be viewed. Thus, television cloud coverage over the globe (Figure 19) is considerably smaller than the radiation data which cover the quasi-globe between 55°N and 55°S (Reference 19).

In the case of TIROS VII, for example, the orbital inclination of 58 degrees leads to a radiation data coverage within nearly the entire zone from 70°N to 70°S, which is approximately 94 percent of the earth's surface; while the television picture coverage each day is less than 15 percent of the globe.

Although the interpretation of the radiation data appears to be complex, it is now becoming possible to introduce this new type of information into practical weather analysis.

Because the radiation data reduction processes presently are accomplished over a period of several weeks, the data are currently available only for research analyses. With suitable modifications and improvements in the computer processing procedures, which appear to be readily attainable, the radiation data should be valuable for weather analyses as well. Data acquired in the 8 to 12 micron region present the most useful synoptic information obtained from the satellite radiation measurements. This information may be interpreted directly to provide details of cloudiness from global to meso-scales on an operational basis.

Future generations of meteorological satellites, such as polar-orbiting and earth-oriented spacecrafts with their larger global data coverage, a considerably simpler scanning geometry, and additional high resolution infrared radiometers, promise an even larger capability for analyses. The various results of this study have attempted to show the principal usefulness and the high degree of applicability of satellite radiation data for worldwide synoptic analysis.

ACKNOWLEDGMENTS

The authors would like to thank Dr. William Nordberg and Mr. William R. Bandeen of the Goddard Space Flight Center; Messrs. Jay S. Winston and P. Krishna Rao of the Meteorological Satellite Laboratory, National Weather Satellite Center, U.S. Weather Bureau; Mr. Kenneth Nagler, Spaceflight Meteorology Group, U.S. Weather Bureau; and Mr. Malcolm Rigby, American Meteorological Society, for their helpful comments and suggestions. We also wish to thank Lt. Col. James C. Sadler, USAF, and Capt. Robert W. Fett, USAF, for their contributions to the analysis herein presented.

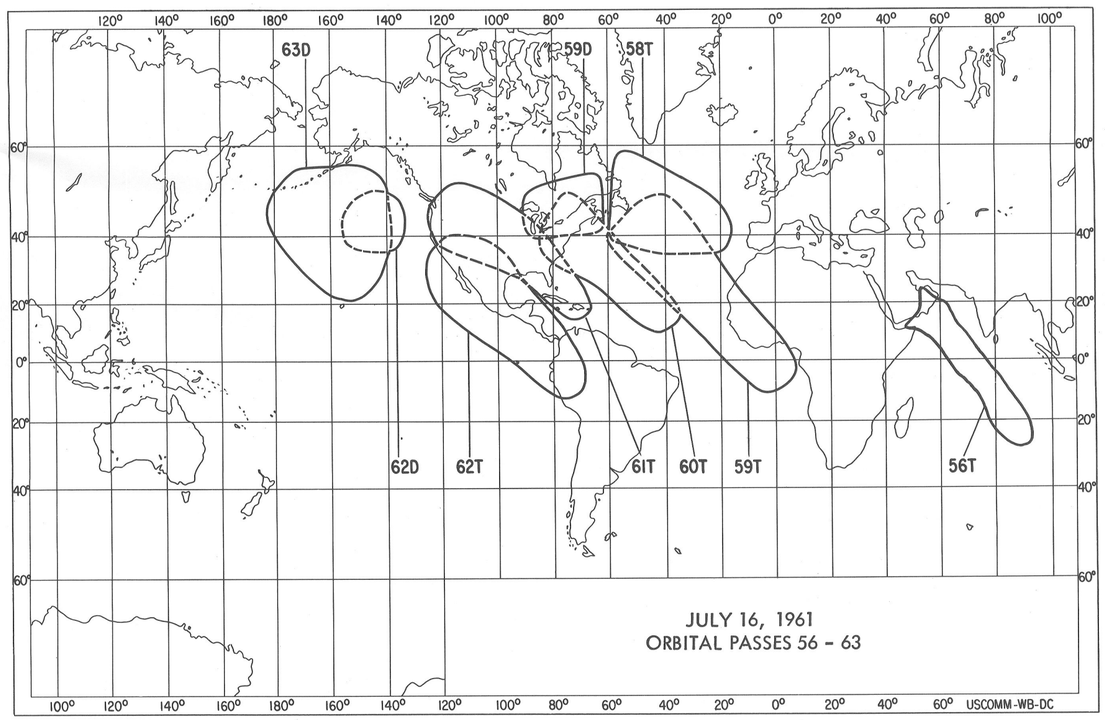

FIGURE 19. Areas of the globe covered by TIROS III television pictures on July 16, 1961.

Page intentionally left blank

REFERENCES

1. "TIROS III Radiation Data User's Manual," NASA Goddard Space Flight Center, August 1962.
2. Fritz, S., and Winston, J. S., "Synoptic Use of Radiation Measurements from Satellite TIROS II," *Monthly Weather Review* 90(1), 1962.
3. Rao, P. K., and Winston, J. S., "An Investigation of Some Synoptic Capabilities of Atmospheric 'Window' Measurements for Satellite TIROS II," *J. Appl. Meteor.* 2(1), 1963.
4. Wark, D. Q., and Winston, J. S., "Application of Satellite Radiation Measurements to Synoptic Analysis and to the Studies of Planetary Heat Budget," *Proceedings of the First International Symposium on Rocket and Satellite Meteorology, 1962;* North Holland Publishing Company; Amsterdam, 1963.
5. "TIROS III Radiation Data Catalog," NASA Goddard Space Flight Center, December 15, 1962.
6. Bandeen, W. R., Samuelson, R. E., and Strange, I. P., "TIROS III Radiation Data Users' Manual Supplement, Correction Models for Instrumental Response Degradation," NASA Goddard Space Flight Center, Greenbelt, Maryland, December 1, 1963.
7. Publications of Synoptic Analyses and/or Data:
   a. Argentine Republic, Servicio Meteorologico Nacional Carta del Tiempo, July–Dec. 1961.
   b. Australia Meteorological Branch, Synoptic Weather Charts, July 1961.
   c. Great Britain Meteorological Office, Daily Weather Report, July–Sept. 1961.
   d. Germany (Federal Republic) Wetterdienst-Taglicher Wetterbericht, July–Sept. 1961.
   e. Greece-Service Meteorologique, Bulletin Quotidien du Temps, July–Sept. 1961.
   f. Indian Meteorological Department, Daily Weather Report, July–Sept. 1961.
   g. International Antarctic Analysis Centre, Melbourne, Australia, Microfilm-analysis and data, July 15–17, 1961.
   h. Japan Meteorological Agency, Daily Weather Maps, July–Sept. 1961.
   i. Mexico, Servicio Meteorologico, Carta del Tiempo, July–Sept. 1961.
   j. New Zealand, Daily Weather Bulletins, July 1961.
   k. Pakistan Meteorological Service, Daily Weather Report, July–Sept. 1961.
   l. South Africa Meteorological Office, Daily Synoptic Charts, July 1961.
   m. Thailand Meteorological Department, Daily Weather Bulletin, May–August 1961.
   n. United Arab Republic, Meteorological Department, Daily Weather Report, July 1961.
   o. United States Weather Bureau, Washington, D.C.
      (1) National Meteorological Center Analyses
      (2) Kunia Forecast Center, Honolulu, Hawaii Analyses
      (3) Northern Hemisphere Data Tabulation—Part II, July 16–17, 1961.
8. Bergeron, T., "General Survey in the Field of Cloud Physics," *International Union of Geodesy and Geophysics, Assoc. Meteor., Ninth General Assembly Memoirs,* Brussels, pp. 120–134, 1951.
9. Boucher, R. J., and Newcomb, R. J., "Synoptic Interpretation of some TIROS Vortex Patterns: A Preliminary Cyclone Model," *J. Appl. Meteor.* 1(2): 127–136, 1962.
10. Serebreny, S. M., Wiegman, E. J., and Hadfield, R. G., "Investigation of the Operational Use of Cloud Photographs from Weather Satellites in the North Pacific," Stanford Research Institute, Menlo Park, California, Final Report, SRI Report 3858, November 1962.
11. Merritt, E. S., "Fleet Applications Meteorological Operational Satellites (Antarctic Area)," Aracon Geophysics Company, Concord, Mass., Final Report, Contract N 189 (188)–56507A, August 15, 1963.
12. Riehl, H., "Waves in the Easterlies and the Polar Front in the Tropics," Dept. of Meteorology, University of Chicago, Misc. Report No. 17, 1943.
13. Palmer, C. E., "Synoptic Analysis over the Southern Ocean," New Zealand Meteorological Office, Prof. Note No. 1, Wellington, N.Z., 1942.
14. Fulks, J. R., "The Instability Line," *Compendium of Meteorology;* Boston: American Met. Society, pp. 647–652, 1951.
15. Sawyer, J. S., "The Structure of the Intertropical Front over N.W. India during the S.W. Monsoon," *Quart. J. Roy. Meteor. Soc.* LXXII: 346–69, 1947.
16. Riehl, H., "Jet Stream," Bureau of Aeronautics, U.S. Navy, 1953.
17. Haurwitz, B., and Austin, J. M., "Climatology;" McGraw Hill Co.: New York, 1944.
18. Fritz, S., "Satellite Pictures and the Origin of Hurricane Anna," *Monthly Weather Review* 90: 507–513, Dec. 1962.
19. "Catalogue of Meteorological Satellite Data—TIROS III. Television Cloud Photography," Key to Meteorological Records Documentation No. 5.33, U.S. Dept. of Commerce, Weather Bureau, 1962.

* U.S. GOVERNMENT PRINTING OFFICE : 1964 O—743-839